



EXTENDED GTN MODEL: MATHEMATICAL ASPECTS AND NUMERICAL STUDY

André Nepomuceno Trajano

University of Brasilia, Faculty UnB at Gama, Área Especial de Indústria Projeção A – Gama, Setor Leste, Brasília/DF, 72444-240
andrenepomuceno@aluno.unb.br

Lucival Malcher

University of Brasilia, Faculty of Tecnology, Department of Mechanical Engineering, Brasília/DF
malcher@unb.br

Guilherme Pacheco

University of Brasilia, Faculty UnB at Gama, Área Especial de Indústria Projeção A – Gama, Setor Leste, Brasília/DF, 72444-240
guilhermepacheco@aluno.unb.br

Carlos Filipe de Queiroz Araújo

University of Brasilia, Faculty UnB at Gama, Área Especial de Indústria Projeção A – Gama, Setor Leste, Brasília/DF, 72444-240
carlosfilipe@aluno.unb.br

Abstract. *In this paper, it is suggested a numerical assessment for the Extended GTN model, which is based on the micromechanical of defects and applied to predominant shear loading conditions. In the first part, theoretical aspects of the GTN model and the extended GTN model are discussed. Furthermore, it is presented an implicit numerical integration algorithm for the extended model, which is based on the operator split methodology and implemented in an academic finite element development. In the second part, numerical tests are carried out regarding the classical GTN model and the Extended GTN model, using shear specimens under pure shear, combined shear/tension and combined shear/compression loading conditions. Aspects as the evolution of the effective damage parameter, evolution of the equivalent plastic strain, the reaction curve, the level of displacement at fracture and ability to predict the correct fracture onset are available.*

Keywords: *micromechanical defects, third invariant, two calibration points*

1. INTRODUCTION

DUCTILE FRACTURE IN METALS is an important subject to be improved in order to predict the correct location of crack initiation in machine components and rupture in general structures. The fracture phenomenon can be studied by its separated evolution contribution as the initiation and growth of general micro defects which is induced by large deformations. Some researchers like McClintock (1968) and Rice & Tracey (1969) developed pioneering work undertaken on the subject, where the nature of defect was taken into account the study of ductile damage by analyzing its geometry in a continuous matrix.

The formulations proposed by Lemaitre and Gurson are the most important coupled damage ductile models to describe the above two methodologies (see Chaboche et al., 2006). Since then, motivated by the limitations of these classical models, such as in prediction of the correct fracture location or in determination of the correct values of the internal variables at fracture, many researchers have proposed improvements in both methodologies, by introducing more effects in the constitutive formulation or in the damage evolution law like the pressure effect, temperature, Lode angle dependence, visco-plastic effects, crack closure effect, shear mechanisms, among others (Tvergaard & Needleman, 1984; Rousselier, 1980 and 2001; Xue, 2007; Nahshon & Hutchinson, 2008; Lemaitre & Chaboche, 1990; Chaboche, 2003; Andrade Pires et al., 2003; Chaboche et al., 2006; Besson, 2010; Mirone et al., 2010; Li et al., 2011; Stoughton et al., 2011; Khan et al., 2012).

These classical coupled damage models have the ability to predict the correct fracture location under a specific range of stress triaxialities (see Xue, 2007; Nahshon & Hutchinson.; 2008; Teng, 2008; Brunig et al, 2013) and are extremely accurate for loading conditions close to the calibration point (see Malcher et al, 2012). For example, within range of high levels of stress triaxialities, where the spherical void growth is the predominant mechanism, the models based on Gurson theory, like the Gurson-Tvergaard-Needleman model, have good performance in prediction of fracture location and parameters in fracture as equivalent plastic strain and displacement. However, under shear dominated loads, where failure is mainly driven by the shear localization of plastic strain of the inter-voids ligaments due to void rotation and distortion, the model does not perform well, (see Engelen et al, 2005; Chaboche et al, 2006).

Motivated by these short comings, in this contribution, a new extension to the GTN model is available, under different loading conditions, in order to analysis the ability to predict the correct fracture location and determinate the internal parameters at fracture.

2. CONSTITUTIVE MODELLING

2.1 Gurson–Tvergaard–Needleman (GTN)'s Model

One of the shortcomings of the Gurson model is the fact that, whatever strain history the material might be subjected; no void volume fraction evolution will be predicted if the initial void ratio is zero. Therefore, in order to enhance the model, several mechanisms for damage nucleation have been proposed such that voids can nucleate depending on the strain history. One of the most well-known nucleation laws was proposed by Chu & Needleman (1980) and later used by Tvergaard–Needleman (1984) in the GTN model. The damage evolution is represented by three simultaneous or successive mechanisms: nucleation, growth and coalescence of voids. The effective porosity, f^* , is determined by the following bilinear function:

$$f^* = \begin{cases} f & , \quad f < f_c \\ f_c + \left(\frac{1}{q_1} - f_c\right) \frac{(f - f_c)}{(f_f - f_c)} & , \quad f \geq f_c \end{cases} \quad (1)$$

where f_c represents the critical void volume fraction and f_f is the void volume fraction at fracture. The effective porosity, f^* , is obtained from both nucleation and growth mechanisms if the void volume fraction is less than the critical value, f_c . The coalescence mechanism becomes active when the void volume fraction is higher than the critical value, f_c . The void volume fraction rate, \dot{f} , is given by the sum of the nucleation and growth mechanism as:

$$\dot{f} = \dot{f}^n + \dot{f}^g. \quad (2)$$

The nucleation mechanism can be driven either by plastic strain or hydrostatic pressure. The definition of the nucleation mechanism based on the equivalent plastic strain is given by:

$$\dot{f}^n = \frac{f_N}{s_N \sqrt{2\pi}} \exp \left[-\frac{1}{2} \left(\frac{\bar{\varepsilon}^p - \varepsilon_N}{s_N} \right)^2 \right] \dot{\bar{\varepsilon}}^p, \quad (3)$$

where f_N represents the volume fraction of all particles with potential for microvoid nucleation, ε_N and s_N are the mean strain/pressure for void nucleation and its standard deviation. The variable $\bar{\varepsilon}^p$ represents the equivalent plastic strain and $\dot{\bar{\varepsilon}}^p$ is the rate of the accumulated plastic strain. The nucleation mechanism only occurs if the hydrostatic pressure is greater than zero, $p > 0$. If the hydrostatic pressure is less or equal to zero, $p \leq 0$, the nucleation rate is equal to zero. The evolution of the growth mechanism in the GTN model is given by the same expression as the original Gurson model (see Gurson, 1977).

The yield function of the GTN's model, which assumes isotropic hardening and isotropic damage, is expressed by:

$$\Phi(\boldsymbol{\sigma}, k, f) = J_2(\boldsymbol{S}) - \frac{1}{3} \left\{ 1 + q_3 f^{*2} - 2q_1 f^* \cosh \left(\frac{q_2 3p}{2\sigma_y} \right) \right\} \sigma_y^2, \quad (4)$$

where parameters q_1 , q_2 and q_3 are introduced to bring the model predictions into closer agreement with full numerical analyses of a periodic array of voids.

2.2 Shear Mechanism

The original formulation of Gurson based models did not include shear effects, which excludes the possibility of predicting shear localization and fracture under conditions of low triaxiality. Under shear dominated loading conditions, the distortion of voids and inter-void linking promotes an effective increase in the material internal degradation and contributes to the material softening. Therefore, in order to improve Gurson based models predictive ability, under both zero and low levels of stress triaxialities, several researchers (Barsoum & Faleskog, 2007a; McVeigh *et al.*, 2007; Xue, 2008; Nahshon & Hutchinson, 2008; Butcher & Chen, 2009; Lecarme *et al.*, 2011; Stoughton *et al.*, 2011) have suggested the introduction of shear effects. The formulation of shear mechanisms, which can be based on geometrical or phenomenological considerations, resulted in evolutions laws that include the influence of the third invariant of the deviatoric stress tensor, the plastic strain tensor and its rate.

The shear damage mechanism proposed by Xue (2007) is can be represented in the rate form as:

$$\dot{D}_{shear} = q_4 f^{q_5} \varepsilon_{eq} \dot{\varepsilon}_{eq}, \quad (5)$$

where q_4 and q_5 are geometrical parameters that can be defined for two or three dimensional problems. For a two dimensional problem, $q_4 = \frac{3}{\sqrt{\pi}}$ and $q_5 = (1/2)$ and for a three dimensional problem, $q_4 = \frac{3}{2} \left(\frac{6}{\pi} \right)^{(1/3)}$ and $q_5 = (1/3)$.

A modified shear damage expression was later derived by Butcher & Chen (2009) that, contrary to Xue (2008), did not perform a Taylor series expansion of the artificial strain and expressed the failure strain with the logarithmic definition as:

$$\dot{D}_{shear} = \frac{1}{\ln \sqrt{1/\chi}} \left(\frac{3\varepsilon_{eq}}{1 + 3\varepsilon_{eq}^2} \right) \dot{\varepsilon}_{eq}. \quad (6)$$

where the parameter χ is the ligament size ratio defined for two or three dimensional problems.

2.3 Lode Angle Function

The shear damage evolutions, which were described for a pure shear loading condition in Section 2.3, need to be generalized for arbitrary stress states. This can be accomplished with the introduction of a Lode angle dependence function. The Lode angle, which is associated to the third invariant of the deviatoric stress tensor, is an essential parameter in the characterization of the effect of the stress state on ductile fracture (Kim *et al.*, 2003 and 2004; Bao and Wierzbicki, 2004; Gao *et al.*, 2006; Barsoum and Faleskog, 2007a and 2007b; Bai and Wierzbicki, 2007; Mirone *et al.*, 2010; Gao *et al.*, 2009:2011; Stoughton *et al.*, 2011; Brüning *et al.*, 2013). The Lode angle dependence function proposed by Xue (2008) is defined by a linear expression of the normalized Lode angle, as:

$$g_0 = 1 - |\bar{\theta}|, \quad (7)$$

where g_0 represents the so-called Lode angle function and $\bar{\theta}$ is the normalized Lode angle, expressed by:

$$\bar{\theta} = 1 - \frac{6|\theta|}{\pi} = 1 - \frac{2}{\pi} \arccos(\xi), \quad (8)$$

where θ represents the Lode angle and ξ is the normalized third invariant, which is a ratio between the third invariant of the deviatoric stress tensor, $r = [(27/2) \cdot \det \mathbf{S}]^{1/3}$, and the von Mises equivalent stress, $q = \sqrt{(3/2)\mathbf{S}:\mathbf{S}}$:

$$\xi = \left(\frac{r}{q} \right)^3. \quad (9)$$

An alternative Lode angle dependence function as been proposed by Nahshon & Hutchinson (2008), which discriminates between uniaxial and biaxial tension and expresses a quadratic relation with the normalized third invariant:

$$g_0 = 1 - \xi^2. \quad (10)$$

Expressions (5) and (6) can be used to activate the shear mechanisms, described in previous sections, whenever shear effects are present.

$$\dot{D}_{shear} = g_0(q_4 f^{q_5} \varepsilon_{eq} \dot{\varepsilon}_{eq}), \quad (11)$$

$$\dot{D}_{shear} = g_0 \left[\frac{1}{\ln \sqrt{1/\chi}} \left(\frac{3\varepsilon_{eq}}{1 + 3\varepsilon_{eq}^2} \right) \dot{\varepsilon}_{eq} \right]. \quad (12)$$

3. EXTENDED CONSTITUTIVE FORMULATION

Due to the limitation of Gurson based models, in the prediction of fracture onset under conditions of low stress triaxiality or capture Mode II and Mode III of crack initiation, several researchers (Barsoum & Faleskog, 2007a; McVeigh *et al.*, 2007; Xue, 2008; Nahshon & Hutchinson, 2008) have proposed the introduction of shear effects (see Section 2.3) on the formulation. Although the results obtained with the modified GTN models (Xue, 2008; Nahshon & Hutchinson, 2008) have shown improvements in the prediction of damage, it has also been observed (Reis *et al.*, 2011; Malcher *et al.*, 2012), that both models have inherent limitations. In particular, the prediction of the location of fracture, the displacement to fracture and the equivalent plastic strain to fracture, for combined stress states, is not adequate. Therefore, in order to overcome these shortcomings, a new extended GTN model is proposed (Malcher *et al.*, 2013) that incorporates a new nucleation law for second-phase particles, the yield surface is modified to include two distinct damage mechanisms (volumetric void growth and shear damage), a modified Lode angle dependence function is introduced and a new criterion for coalescence is proposed.

3.1 Nucleation mechanism

The extended GTN model, proposed by Malcher *et al.* (2013), incorporates two independent nucleation mechanisms. The first one, which is the conventional nucleation mechanism of the GTN model, triggers the evolution of the void volume fraction. The second triggers the evolution of the shear mechanism. The activation of these nucleation mechanisms under pure volumetric and shear conditions is relatively straightforward to establish.

Nevertheless, under arbitrary stress states that may include combinations of tensile/shear or compressive/shear is not so easy to define. It is necessary to couple both mechanisms and also establish their relative magnitude, as:

$$\dot{f}^n = (1 - g_0) \frac{f_N}{s_N \sqrt{2\pi}} \exp \left[-\frac{1}{2} \left(\frac{\bar{\varepsilon}^p - \varepsilon_N}{s_N} \right)^2 \right] \dot{\varepsilon}^p, \quad (13)$$

$$\dot{D}^n = g_0 \frac{D_N}{s'_N \sqrt{2\pi}} \exp \left[-\frac{1}{2} \left(\frac{\bar{\varepsilon}^p - \varepsilon'_N}{s'_N} \right)^2 \right] \dot{\varepsilon}^p. \quad (14)$$

Under pure tensile loading conditions, the function g_0 is equal to zero and only primary nucleation of voids occurs (Equation 13). For pure shear loading conditions, the function g_0 is equal to one and only secondary nucleation occurs (Equation 14). For combined tensile/shear stress states, both mechanisms are active and the Lode angle function defines the relative importance of each component. Finally, if a combination of shear/compressive conditions is present there is no nucleation of primary voids and secondary nucleation takes place with the function g_0 defining the relative magnitude.

3.2 Incorporation shear effects

In contrast with original approach, Malcher *et al* (2013) have proposed the use of two separate damage variables. The first one is the evolution of the void volume fraction employed in the GTN model, rewritten here with appropriate modifications, as:

$$\dot{f} = \dot{f}^n + \dot{f}^g = (1 - g_0) \frac{f_N}{s_N \sqrt{2\pi}} \exp \left[-\frac{1}{2} \left(\frac{\bar{\varepsilon}^p - \varepsilon_N}{s_N} \right)^2 \right] \dot{\varepsilon}^p + (1 - f) \dot{\varepsilon}_v^p. \quad (15)$$

The second variable is the evolution of damage due to shear effects, which is defined by an independent scalar variable, as:

$$\dot{D} = \dot{D}^n + q_6 \dot{D}^{shear} = g_0 \frac{D_N}{s'_N \sqrt{2\pi}} \exp \left[-\frac{1}{2} \left(\frac{\bar{\varepsilon}^p - \varepsilon'_N}{s'_N} \right)^2 \right] \dot{\varepsilon}^p + q_6 \dot{D}^{shear}, \quad (16)$$

where \dot{D} represents the evolution of the shear damage variable, \dot{D}^n represents its nucleation, which was introduced in Equation (14), and \dot{D}^{shear} is the evolution of shear effects that can be defined based on geometrical considerations (see Equations (11) and (12)) or phenomenological considerations (Nahshon & Hutchinson, 2008). The parameter q_6 is a numerical constant, calibrated for each specific material, which defines the magnitude of the damage growth rate in shear.

The extended GTN model proposed here has two scalar damage variables: a volumetric damage component characterized by the void volume fraction, f , and a deviatoric damage component described by shear damage, D . Each of these variables will be coupled with a specific component of the stress tensor: the hydrostatic pressure, p , will be related with the void volume fraction, f and the deviatoric component of the stress tensor, \mathbf{S} , will be associated with the shear damage variable, D . The yield function of the model is therefore, defined by the following equation:

$$\Phi(\boldsymbol{\sigma}, k, f, D) = \frac{J_2(\mathbf{S})}{(1 - D)} - \frac{1}{3} \left\{ 1 + q_3 f^2 - 2q_1 f \cosh \left(\frac{q_2 3p}{2\sigma_y} \right) \right\} \sigma_y^2. \quad (17)$$

In Box 1, the basic constitutive equations and evolution laws for the internal variables and damage are summarized:

Box 1. GTN's extended modified model including nucleation, growth and shear effects.

(i) Elasto-plastic split of the strain tensor

$$\boldsymbol{\varepsilon} = \boldsymbol{\varepsilon}^e + \boldsymbol{\varepsilon}^p$$

(ii) Elastic law

$$\boldsymbol{\sigma} = \mathbb{D}^e : \boldsymbol{\varepsilon}^e$$

(iii) Yield function

$$\Phi(\boldsymbol{\sigma}, r, f, D) = \frac{J_2}{1-D} - \frac{1}{3} \left[1 + q_3 f^2 - 2q_1 f \cosh\left(\frac{3q_2 p}{2\sigma_y}\right) \right] \sigma_y^2$$

(iv) Plastic flow and evolution equations for R , f and D

$$\dot{\boldsymbol{\varepsilon}}^p = \dot{\gamma} \mathbf{N}$$

$$\dot{R} = -\dot{\gamma} \frac{\partial \Phi}{\partial k}$$

$$\dot{f} = (1 - g_0) \frac{f_N}{S_N \sqrt{2\pi}} \exp\left[-\frac{1}{2} \left(\frac{\bar{\varepsilon}^p - \varepsilon_N}{S_N}\right)^2\right] \dot{\boldsymbol{\varepsilon}}^p + (1 - f) \dot{\varepsilon}_v^p$$

$$\dot{D} = g_0 \frac{D_N}{S'_N \sqrt{2\pi}} \exp\left[-\frac{1}{2} \left(\frac{\bar{\varepsilon}^p - \varepsilon'_N}{S'_N}\right)^2\right] \dot{\boldsymbol{\varepsilon}}^p + [g_0]^{|\eta|+k} q_6 \dot{D}^{shear}$$

where,

$$\dot{D}^{shear} = \begin{cases} q_3 D^{q_4} \bar{\varepsilon}^p \cdot \dot{\boldsymbol{\varepsilon}}^p & , \quad \text{if Xue's shear mechanism is chosen} \\ \frac{1}{\ln \sqrt{1/\chi}} \left(\frac{3\bar{\varepsilon}^p}{1 + 3\bar{\varepsilon}^{p2}} \right) \dot{\boldsymbol{\varepsilon}}^p & , \quad \text{if Butcher's shear mechanism is chosen} \end{cases}$$

$$g_0 = \begin{cases} 1 - |\bar{\theta}| & , \quad \text{if Xue's Lode angle dependence function is chosen} \\ 1 - \xi^2 & , \quad \text{if Nahshon's Lode angle dependence function is chosen} \end{cases}$$

and,

$$\dot{\varepsilon}_v^p = \sqrt{\frac{2}{3}} (\dot{\boldsymbol{\varepsilon}}^p : \dot{\boldsymbol{\varepsilon}}^p) \quad \dot{\varepsilon}_v^p = \text{tr}(\dot{\boldsymbol{\varepsilon}}^p)$$

(v) Loading/unloading criterion

$$\dot{\gamma} \geq 0, \quad \Phi \leq 0, \quad \dot{\gamma} \Phi = 0$$

4. NUMERICAL INTEGRATION ALGORITHM

In this section, the numerical solution strategy adopted to perform the numerical simulations is summarized. Algorithms based on operator split methodology are especially suitable for the numerical integration of the evolution problem and have been widely used in computational plasticity (see Simo & Hughes, 1998; De Souza Neto *et al.*, 2008). The overall algorithm for numerical integration is summarized in Box 2.

Box 2. Fully implicit Elastic predictor/Return mapping algorithm.

(i) Evaluate the elastic trial state: Given the incremental strain Δ and the state variables at t_n :

$$\begin{aligned} \boldsymbol{\varepsilon}_{n+1}^{e\ trial} &= \boldsymbol{\varepsilon}_n^e + \Delta\boldsymbol{\varepsilon} & ; & & \bar{\boldsymbol{\varepsilon}}_{n+1}^{p\ trial} &= \bar{\boldsymbol{\varepsilon}}_n^p & ; & & R_{n+1}^{trial} &= R_n \\ f_{n+1}^{trial} &= f_n & ; & & D_{n+1}^{trial} &= D_n & ; & & \mathbf{S}_{n+1}^{trial} &= 2G\boldsymbol{\varepsilon}_{n+1}^{e\ trial} \\ p_{n+1}^{trial} &= K\varepsilon_{v\ n+1}^{e\ trial} & ; & & \sigma_y^{trial} &= \sigma_y(R_{n+1}^{trial}) \end{aligned}$$

(ii) Check plastic admissibility:

$$\text{IF } \Phi^{trial} = \frac{J_2^{trial}}{1-D_{n+1}^{trial}} - \frac{1}{3} \left[1 + q_3 f_{n+1}^{trial 2} - 2q_1 f_{n+1}^{trial} \cosh\left(\frac{3q_2 p_{n+1}^{trial}}{2\sigma_y^{trial}}\right) \right] (\sigma_y^{trial})^2 \leq 0 \text{ THEN}$$

Set $(\cdot)_{n+1} = (\cdot)_{n+1}^{trial}$ (**elastic step**) and go to (v)

ELSE go to (iii)

(iii) Return mapping (**plastic step**): Solve the system of equations for $\Delta\gamma, p_{n+1}, f_{n+1}, R_{n+1}$ and D_{n+1}

$$\left\{ \begin{array}{l} \frac{J_2^{trial}}{\left[1 + \left(\frac{2G\Delta\gamma}{1-D_{n+1}}\right)^2\right]^2 (1-D_{n+1})} - \frac{1}{3} \left[1 + q_3 f_{n+1}^{trial 2} - 2q_1 f_{n+1}^{trial} \cosh\left(\frac{3q_2 p_{n+1}}{2\sigma_y}\right) \right] \sigma_y^2 \\ p_{n+1} - p_{n+1}^{trial} + \Delta\gamma K \sigma_y q_1 q_2 f_{n+1} \sinh\left(\frac{3q_2 p_{n+1}}{2\sigma_y}\right) \\ f_{n+1} - f_{n+1}^{trial} - \Delta f^n - \Delta f^g \\ R_{n+1} - R_{n+1}^{trial} - \Delta R \\ D_{n+1} - D_{n+1}^{trial} - \Delta D^n - q_6 \Delta D^{shear} \end{array} \right\} = \left\{ \begin{array}{l} 0 \\ 0 \\ 0 \\ 0 \\ 0 \end{array} \right\}$$

where,

$$\begin{aligned} \Delta f^n &= (1 - g_{0\ n+1}) \frac{f_N}{S_N \sqrt{2\pi}} \exp\left[-\frac{1}{2} \left(\frac{\bar{\boldsymbol{\varepsilon}}_{n+1}^p - \boldsymbol{\varepsilon}_N}{S_N}\right)^2\right] \Delta \bar{\boldsymbol{\varepsilon}}^p \\ \Delta f^g &= (1 - f_{n+1}) \Delta\gamma \sigma_y q_1 q_2 f_{n+1} \sinh\left(\frac{3q_2 p_{n+1}}{2\sigma_y}\right) \\ \Delta R &= \frac{\Delta\gamma}{(1 - f_{n+1} - D_{n+1})} \left\{ q_1 q_2 f_{n+1} p_{n+1} \sinh\left(\frac{3q_2 p_{n+1}}{2\sigma_y}\right) \right. \\ &\quad \left. + \frac{2}{3} \sigma_y \left[1 + q_3 f_{n+1}^2 - 2q_1 f_{n+1} \cosh\left(\frac{3q_2 p_{n+1}}{2\sigma_y}\right) \right] \right\} \end{aligned}$$

Box 2. Fully implicit Elastic predictor/Return mapping algorithm (continue).

$$\Delta D^n = g_{0\ n+1} \frac{D_N}{S'_N \sqrt{2 \cdot \pi}} \exp \left[-\frac{1}{2} \left(\frac{\bar{\varepsilon}_{n+1}^p - \varepsilon'_N}{S'_N} \right)^2 \right] \Delta \bar{\varepsilon}^p$$

ΔD^{shear}

$$= \begin{cases} [g_{0\ n+1}]^{\left(\frac{1}{|\eta_{n+1}|+k}\right)} q_4 D_{n+1}^{q_5} \bar{\varepsilon}_{n+1}^p \Delta \bar{\varepsilon}^p & , \text{ if Xue's mechanism is chosen} \\ [g_{0\ n+1}]^{\left(\frac{1}{|\eta_{n+1}|+k}\right)} \frac{1}{\ln \sqrt{1/\chi}} \left(\frac{3 \bar{\varepsilon}_{n+1}^p}{1 + 3 \bar{\varepsilon}_{n+1}^p} \right) \cdot \Delta \bar{\varepsilon}^p & , \text{ if Butcher's mechanism is chosen} \end{cases}$$

$$g_{0\ n+1} = (1 - \xi_{n+1}^2)$$

$$\chi = \begin{cases} \left(\frac{4}{\pi} D_{n+1} \frac{\lambda_2}{\lambda_1} \right)^{\frac{1}{2}}, & \text{ if 2D problem} \\ \left(\frac{6}{\pi} D_{n+1} \frac{\lambda_2}{\lambda_1} \right)^{\frac{1}{3}}, & \text{ if 3D problem} \end{cases}$$

(iv) Update the others state variables:

$$\boldsymbol{\varepsilon}_{n+1}^e = \boldsymbol{\varepsilon}_{n+1}^{e\ trial} - \Delta \gamma \left[\frac{\mathbf{s}_{n+1}^{trial}}{\left[1 + \left(\frac{2G\Delta\gamma}{1 - D_{n+1}} \right) \right] (1 - D_{n+1})} + \frac{1}{3} \sigma_y q_1 q_2 f_{n+1} \sinh \left(\frac{3q_2 p_{n+1}}{2\sigma_y} \right) \mathbf{I} \right]$$

$$\mathbf{s}_{n+1} = \frac{\mathbf{s}_{n+1}^{trial}}{\left[1 + \left(\frac{2G\Delta\gamma}{1 - D_{n+1}} \right) \right]}$$

$$\boldsymbol{\sigma}_{n+1} = \mathbf{s}_{n+1} + p_{n+1} \mathbf{I}$$

$$\Delta \bar{\varepsilon}^p = \Delta \gamma \sqrt{\frac{2}{3} \left\{ \frac{\mathbf{s}_{n+1}^{trial} \cdot \mathbf{s}_{n+1}^{trial}}{\left[1 + \left(\frac{2G\Delta\gamma}{1 - D_{n+1}} \right) \right]^2 (1 - D_{n+1})^2} + \frac{1}{3} \left[\sigma_y q_1 q_2 f_{n+1} \sinh \left(\frac{3q_2 p_{n+1}}{2\sigma_y} \right) \right]^2 \right\}}$$

$$\bar{\varepsilon}_{n+1}^p = \bar{\varepsilon}_{n+1}^{p\ trial} + \Delta \bar{\varepsilon}^p$$

(v) Exit

5. NUMERICAL RESULTS

For a consistent analysis of the proposed formulation at low level of stress triaxiality, some numerical tests are performed using the butterfly specimen and the implicit algorithm suggested in above sections. Three different loading conditions are taken as: pure shear, shear/tensile and shear/compression, and two materials as: aluminum alloy 2024-T351 and steel 1045. The performance of some parameters as equivalent plastic strain and displacement at fracture as well as the ability to predict the correct fracture location are evaluated. At the end, the numerical results determined by

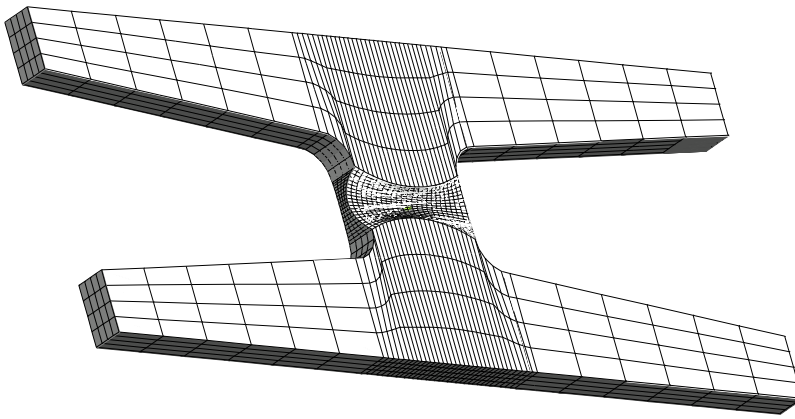


Figure 2. Finite elements mesh for butterfly specimen.

5.2 Evolution of equivalent plastic strain and damage parameters

The experimental results obtained by Bai (2008), which will be used as reference for comparison, are listed in Table 3. In particular, the displacement at fracture, u_f , the equivalent strain at fracture, $\bar{\epsilon}_f$, and the location of crack initiation are listed for each loading condition and material.

Table 3: Reference values for different loading scenarios of two materials.

Angle	Aluminum alloy 2024-T351			Steel 1045		
	u_f	$\bar{\epsilon}_f$	Fracture location	u_f	$\bar{\epsilon}_f$	Fracture location
0°	0.70	0.22	Surface of the critical zone	1.03	0.50	Surface of the critical zone
10°	0.50	0.26	Middle of the critical zone	0.42	0.36	Middle of the critical zone
-5°	1.00	0.22	Surface of the critical zone	1.71	0.60	Surface of the critical zone

Based on numerical results presented, we can conclude that the new formulation has the ability to predict the correct moment to crack formation by appropriately calibrating the numerical constants and parameters of the model. Both the equivalent plastic strain and the displacement, calculated by present formulation, are in close agreement with the experimental data for both loading conditions and materials applied (see Table 4 and Table 5).

Table 4: Numerical results for butterfly specimen using 1045 steel and different loading conditions.

Angle	Experimental data			Numerical results					
	u_f	$\bar{\epsilon}^p$	q_6	u_f	$\bar{\epsilon}^p$	η_{av}	θ_{av}	f	d
0°			0.5	1.03	0.516	0.022	0.061	0.000	0.122
	1.03	0.50	1.0	1.03	0.522	0.022	0.060	0.000	0.160
			1.5	1.03	0.528	0.021	0.057	0.000	0.204
10°			0.5	0.33	0.257	0.241	0.477	0.018	0.045
	0.42	0.36	1.0	0.44	0.353	0.245	0.485	0.026	0.053
			1.5	0.59	0.440	0.257	0.507	0.030	0.061
-5°			0.5	1.71	0.611	-0.066	-0.173	0.000	0.100
	1.71	0.60	1.0	1.71	0.612	-0.065	-0.173	0.000	0.126
			1.5	1.71	0.616	-0.065	-0.173	0.000	0.153

Table 5: Numerical results for butterfly specimen using aluminum 2024-T351 alloy and different loading conditions.

Angle	Experimental data		Numerical results						
	u_f	$\bar{\varepsilon}^p$	q_6	u_f	$\bar{\varepsilon}^p$	η_{av}	θ_{av}	f	d
0°	0.70	0.22	1.0	0.70	0.292	0.018	0.048	0.000	0.084
			2.0	0.70	0.298	0.017	0.048	0.000	0.107
			3.0	0.70	0.305	0.017	0.047	0.000	0.137
			4.0	0.70	0.318	0.017	0.046	0.000	0.179
10°	0.50	0.26	1.0	0.55	0.230	0.250	0.486	0.013	0.032
			2.0	0.63	0.271	0.254	0.492	0.017	0.039
			3.0	0.75	0.336	0.257	0.494	0.021	0.051
			4.0	0.75	0.337	0.264	0.502	0.021	0.056
-5°	1.00	0.22	1.0	1.00	0.414	-0.066	-0.176	0.000	0.084
			2.0	0.98	0.424	-0.065	-0.173	0.000	0.110
			3.0	0.95	0.432	-0.064	-0.169	0.000	0.140
			4.0	0.93	0.455	-0.063	-0.165	0.000	0.190

5.3 Prediction of the correct fracture location

Figures 3 and 4 present the contour of effective damage for the steel 1045 and the aluminum alloy 2024-T351, respectively, at fracture. It is possible to conclude that the new damage formulation has the ability to predict the correct fracture location in all loading conditions.

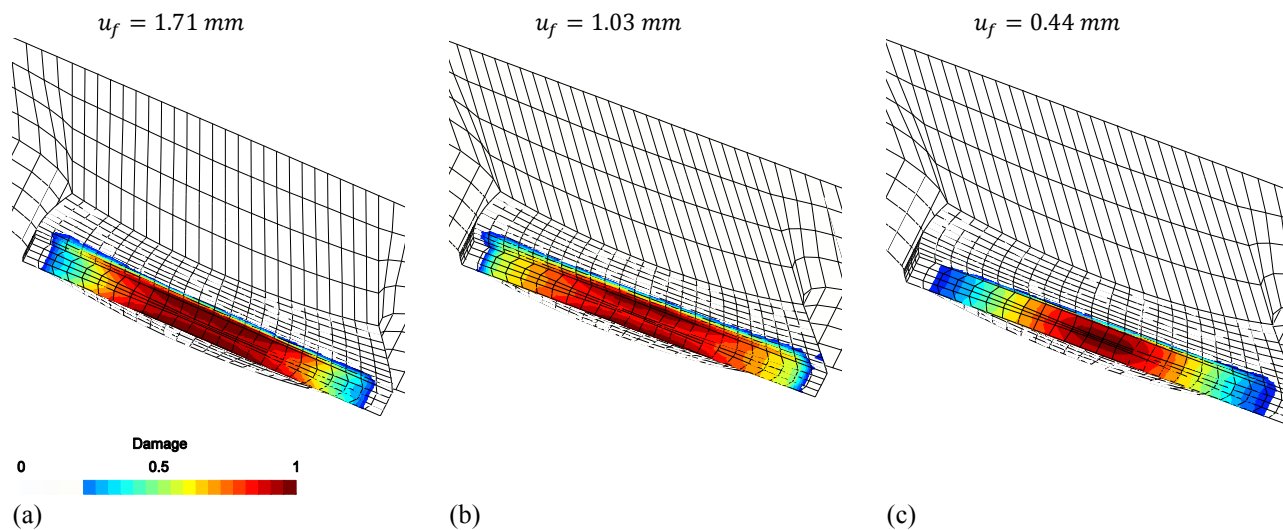


Figure 3. Effective damage contour for butterfly specimen using 1045 steel. (a) shear/compression, (b) pure shear and (c) shear/tensile loading conditions.

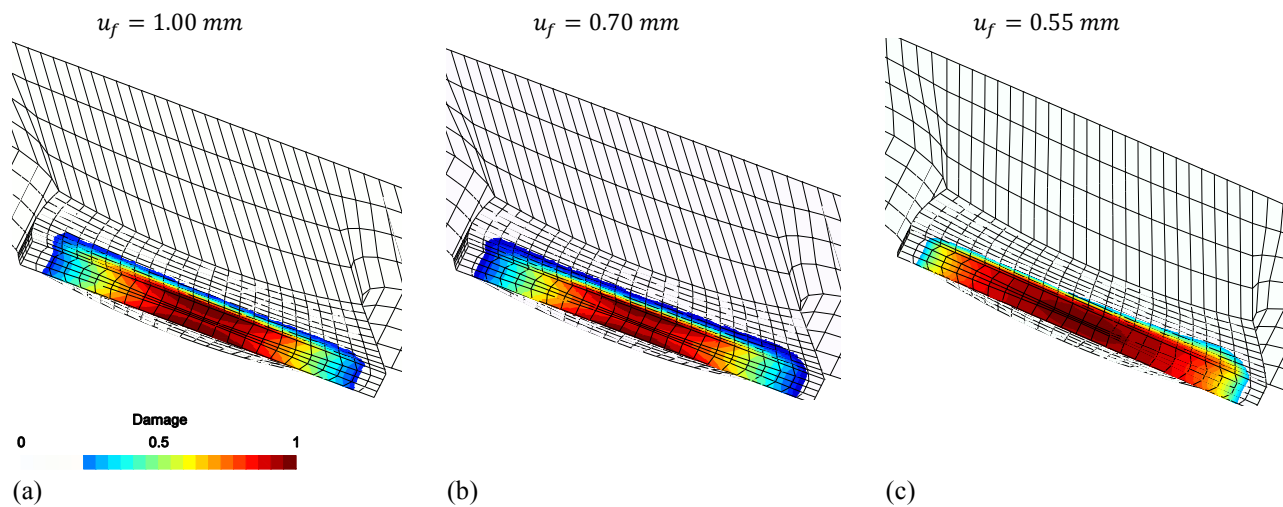


Figure 4. Effective damage contour for butterfly specimen using aluminum 2024-T351 alloy. (a) shear/compression, (b) pure shear and (c) shear/tensile loading conditions.

6. CONCLUSION

In this contribution, a new formulation was tested, regarding the ability to predict ductile fracture under a low level of stress triaxiality. Numerical tests were conducted, with an implicit integration algorithm, in order to evaluate the formulation ability to predict the crack formation. A butterfly specimen was employed and two different materials: the steel 1045 and the aluminum alloy 2024-T351 were used. In all loading conditions, the model behaves well, either in the determination of the correct level of equivalent plastic strain and displacement at fracture, or in prediction of the location of crack formation.

The introduction of two damage parameters affecting separate components of the stress tensor stress critically affects the evolution of internal variables and allows more accurate values at the time of crack formation. Furthermore, the introduction of a new micro-defects nucleation mechanism facilitates the calibration model and thus an improved performance for a wide range of stress triaxiality. The introduction of the stress triaxiality dependence in the evolution of shear damage parameter also enhanced the prediction of the fracture location under combined loading conditions, since this parameter influences the behavior of material under low stress triaxiality. An effective damage variable is determined in post-processed step as a function of both volume void fraction and shear damage parameter. A penalization factor is introduced in order to accelerate the damage evolution due to the presence of multi axial loading conditions.

In spite of the best performance of this formulation when compared to the models available in the literature, the introduction of more parameters that need to be calibrated requires special attention. In particular, two calibration points are required to fully define the model. A calibration point at high triaxiality, which was already required in GTN original model, and now a new point at low triaxiality, to obtain the parameters that govern the new shear damage evolution law. In summary, the new model was formulated in order to perform well in all loading conditions and for different materials. From the results presented, it is possible to conclude that the objective was achieved for the cases tested.

7. REFERENCES

- Andrade Pires, F.M., César de Sá, J.M.A., Costa Sousa, L., Natal Jorge, R.M. (2003). Numerical Modelling of ductile plastic damage in bulk metal forming, *International Journal of Mechanical Sciences*, 45:273–294.
- Bai, Y., Wierzbicki, T. (2007). A new model of metal plasticity and fracture with pressure and Lode dependence, *International Journal of Plasticity*, 24:1071-1096.
- Bai, Y. (2008). Effect of Loading History on Necking and Fracture. Ph.D Thesis, Massachusetts Institute of Technology.
- Bao, Y., Wierzbicki, T. (2004). On fracture *locus* in the equivalent strain and stress triaxiality space. *International Journal of Mechanical Sciences*. 46 (81):81-98.
- Barsoum, I., Faleskog, J. (2007a). Rupture in combined tension and shear: experiments. *International Journal of Solids and Structures*, 44:1768–1786.
- Barsoum, I., Faleskog, J. (2007b). Rupture in combined tension and shear: micromechanics. *International Journal of Solids and Structures*, 44:5481–5498.
- Besson, J., (2010). Continuum Models of Ductile Fracture: A Review. *International Journal of Damage Mechanics*, 19:3-52.

- Brünig, M., Gerke, S., Hagenbrock, V., (2013). Micro-mechanical studies on the effect of the stress triaxiality and the Lode parameter on ductile damage. *International Journal of Plasticity*, In Press, Accepted Manuscript.
- Butcher, C., Chen, Z., Bardelcik, A., Worswick M., (2009). Damage-based finite-element modeling of tube hydroforming. *International Journal of Fracture*, 155:55–65.
- Chaboche, J.L. (2003). Damage mechanics. In: Milne, I., Ritchie, R.O. and B. Karihaloo (eds.) *Comprehensive Structural Integrity*, vol. 2. Elsevier-Pergamon, pp. 213–284.
- Chaboche, J.L., Boudifa, M., Saanouni, K., (2006). A CDM approach of ductile damage with plastic compressibility. *International Journal of Fracture*, 137:51–75.
- De Souza Neto, E.A., Peri'c, Owen, D.R.J. (2008). *Computational methods for plasticity: theory and applications*. John Wiley & Sons Ltd.
- Engelen, Roy A.B. (2005). *Plasticity-induced Damage in Metals / nonlocal modelling at finite strains*. PhD Thesis – Eindhoven : Technische Universiteit Eindhoven.
- Gao, X., Kim, J., (2006). Modeling of ductile fracture: significance of void coalescence. *Int. J. Solids Struct.* 43, 6277–6293.
- Gao, X., Zhang, G., Roe, C., (2009). A study on the effect of the stress state on ductile fracture. *Int. J. Damage Mech.*, 19, 75–94.
- Gao, X., Zhang, T., Zhou, J., Graham, S.M., Hayden, M., Roe, C. (2011), On stress-state dependent plasticity modeling: Significance of the hydrostatic stress, the third invariant of stress deviator and the non-associated flow rule, *International Journal of Plasticity*, vol. 27, 2:217-231.
- Gurson, A.L. (1977). Continuum Theory of ductile rupture by void nucleation and growth - Part I. Yield criteria and flow rules for porous ductile media. *J. Engrg. Mat. Tech.*, 99:2-15.
- Khan, A. S., Liu, H. (2012). A new approach for ductile fracture prediction on Al 2024-T351 alloy. *International Journal of Plasticity* 35, 1–12.
- Kim, J., Gao, X., Srivatsan, T.S., (2003). Modeling of crack growth in ductile solids: a three-dimensional analysis. *Int. J. Solids Struct.* 40, 7357–7374.
- Kim, J., Gao, X., Srivatsan, T.S., (2004). Modeling of void growth in ductile solids: effects of stress triaxiality and initial porosity. *Eng. Frac. Mech.* 71, 379–400.
- Lecarme, L., Tekoglu, C., Pardoen, T., (2011). Void growth and coalescence in ductile solids with stage III and stage IV strain hardening. *International Journal of Plasticity* 27, 1203–1223.
- Lemaitre, J. (1984). How to Use Damage Mechanics. *Nuclear Engrg. Design*, 80, 233–245.
- Lemaitre, J. (1985). A continuous damage mechanics model for ductile fracture. *Journal of Engineering Materials and Technology - Trans. of the ASME*, 107:83–89.
- Lemaitre, J., Chaboche, J.L. (1990). *Mechanics of Solid Materials*. Cambridge Univ. Press.
- Li, H., Fu, M.W., Lu, J., Yang, H., (2011). Ductile fracture: experiments and computations. *International Journal of Plasticity*, 27, pp. 147–180
- Malcher, L. ; Andrade Pires, F.M. ; César de Sá, J.M.A ; Andrade, F.X.C . (2009). Numerical integration algorithm of a new model for metal plasticity and fracture including pressure and Lode angle dependence. *International Journal of Material Forming - Springer*, 2:443-446.
- Malcher, L. ; Andrade Pires, F.M. ; César de Sá, J.M.A., (2012), An Assessment of Isotropic Damage Constitutive Models under High and Low Stress Triaxialities. *International Journal of Plasticity*.
- McClintock, F. A. (1968). A Criterion for Ductile Fracture by the Growth of Holes. *J. Appl. Mech.*, 35, 363–371.
- McVeigha, C., Vernereya, F., Liu, W.K., Moran, B., Olson, G. (2007). An Interactive Micro-Void Shear Localization Mechanism in High Strength Steels. *Journal of the Mechanics and Physics of Solids*, 55, 225–244.
- Mirone, G., Corallo, D., (2010). A local viewpoint for evaluating the influence of stress triaxiality and Lode angle on ductile failure and hardening. *International Journal of Plasticity* 26, 348–371.
- Nahshon, K., Hutchinson, J. (2008). Modification of the Gurson model for shear failure. *European Journal of Mechanics A/Solids*, 27:1–17.
- Reis, F.J.P.; Malcher, L. ; Andrade Pires, F.M. ; César de Sá, J.M.A., (2010), A modified GTN model for the prediction of ductile fracture at low stress triaxialities. *International Journal of Structural Integrity*
- Rice, J. R., Tracey, D., M. (1969). On the ductile enlargement of voids in triaxial stress fields. *Journal of the Mechanics and Physics of Solids*, 17:201–217.
- Rousselier's, G. (1980). Finite deformation constitutive relations including ductile fracture damage. In: Nemat-Nasser (ed.) *Three-Dimensional Constitutive Relations and Ductile Fracture*. North-Holland Publ. Comp., 1981 pp. 331–355.
- Rousselier's, G. (2001). The Rousselier model for porous metal plasticity and ductile fracture. In: Lemaitre, J. (ed.) *Handbook of Materials Behavior Models*, vol. 2. Academic Press, New York, chapter 6.6, pp. 436–445.
- Simo, J.C., & Hughes, T.J.R. (1998). *Computational Inelasticity*. New York: Springer-Verlag.
- Stoughton, T. B., Yoon, J. W., (2011). A new approach for failure criterion for sheet metals. *International Journal of Plasticity*, 27, 440–459.
- Teng, X. (2008). Numerical prediction of slant fracture with continuum damage mechanics. *Engineering Fracture*

22nd International Congress of Mechanical Engineering (COBEM 2013)
November 3-7, 2013, Ribeirão Preto, SP, Brazil

Mechanics, 75:2020–2041.

Tvergaard, V. and Needleman, A. (1984). Analysis of the cup-cone fracture in a round tensile bar. *Acta Met.* 32:157–169.

Xue, L. (2007). *Ductile Fracture Modeling – Theory, Experimental Investigation and Numerical Verification*, Ph.D Thesis, Massachusetts Inst. of Technology.

Xue, L. (2008). Constitutive modeling of void shearing effect in ductile fracture of porous materials. *Engineering Fracture Mechanics*, 75: 3343–3366.

8. RESPONSIBILITY NOTICE

The authors are the only responsible for the printed material included in this paper.